H2+ formation from H2O+ mediated by the core-excitation-induced nuclear motion in H2O

H_2^+ formation from H_2O^+ mediated by the core-excitation-induced nuclear motion in H_2O

A. Hiraya,[1] K. Nobusada,[2] M. Simon,[3,4] K. Okada,[5] T. Tokushima,[1] Y. Senba,[1] H. Yoshida,[1] K. Kamimori,[1] H. Okumura,[6] Y. Shimizu,[7] A.-L. Thomas,[4] P. Millie,[4] I. Koyano,[6] and K. Ueda[7,*]

[1]*Department of Physical Sciences, Hiroshima University, Higashi-Hiroshima 739-8526, Japan*
[2]*Division of Chemistry, Graduate School of Science, Hokkaido University, Sapporo, Hokkaido 060-0810, Japan*
[3]*LURE, Batiment 209d, Université Paris–Sud, 91405 Orsay Cedex, France*
[4]*CEA/DRECAM/SPAM and Laboratoire Francis Perrin, CEN Saclay, 91191 Gif/Yvette Cedex, France*
[5]*Department of Chemistry, Hiroshima University, Higashi-Hiroshima 739-8526, Japan*
[6]*Department of Material Science, Himeji Institute of Technology, Kamigori, Hyogo 678-1297, Japan*
[7]*Research Institute for Scientific Measurements, Tohoku University, Sendai 980-8577, Japan*

The vibrational structure of the O $1s^{-1}2b_2$ core-excited state of H_2O is observed and ascribed to the mixture of symmetric stretching and bending motions with a_1 symmetry. The formation of H_2^+ is found to increase linearly with an increase in energy stored in the nuclear motion of the O $1s^{-1}2b_2$ state, demonstrating that this dissociation channel is mediated by the nuclear motion in the core-excited state. The reaction pathway to the H_2^+ formation along the Auger final state of H_2O^+, mediated by the nuclear motion before the Auger decay, is discussed with the help of *ab initio* potential surfaces of the Auger final states.

I. INTRODUCTION

The progress in the techniques for generation and mono-chromatization of synchrotron radiation in the soft-x-ray region has been remarkable in the last decade and now one can promote any core electron to a specific quantum state using a narrow-band soft-x-ray beam and investigate the relaxation dynamics of the core-excited quantum state in detail. The core-excited state in general relaxes via very fast electronic decay with a time scale of the order of 10 fs emitting an Auger electron. Within this very short time scale, however, the nuclear motion can proceed in the core-excited state. Both high-resolution absorption (excitation) spectroscopy [1–3] and electron emission (deexcitation) spectroscopy [4–8] have been successfully applied to probe the nuclear motion in the core-excited states. So, it is now well understood that dissociation begins along the potential surface of the core-excited state before the Auger decay and finishes along the potential surface of the Auger final state. Because of the specific shape of the potential surface of the core-excited state, a specific dissociation channel such as site-specific fragmentation may be opened by the core excitation [9,10]. It is thus particularly interesting to investigate the influence of the nuclear motion in the core-excited state onto the dissociation process because such investigations may give us a clue to controlling a specific reaction channel. Such investigations are, however, still rare [11,12] and to our knowledge there are no such reports where vibronic quantum states are actually resolved in the core-excited state.

In this paper we report the observation of a dissociation channel mediated by the vibrational motion in the core-excited state. The sample molecule used here is H_2O and

H_2^+ formation is observed as a function of vibrational quantum numbers in the core-excited state. H_2^+ formation from H_2O^+ via the core-excitation of H_2O was first observed by Piancastelli *et al.* [13]. They suggested a key role of the bending motion in the core-excited state, though they did not resolve the vibrations at their limited resolution. In the present study vibrations in the core-excited state are resolved and better evidence is presented for the role of the vibrations in the core-excited state: it is demonstrated that the rate for the H_2^+ formation increases linearly with the increase in the vibrational energy stored in the core-excited state.

The H_2O molecule has the C_{2v} symmetry structure [$r(O—H)=0.958$ Å; $\theta_{H—O—H}=104.4°$] in the ground state and the electronic configuration is

$$1a_1^2 2a_1^2 1b_2^2 3a_1^2 1b_1^2; 4a_1^0 2b_2^0 (^1A_1).$$

Here $1a_1$ and $2a_1$ are O $1s$ and O $2s$ orbitals, respectively. The outermost orbital $1b_1$ has mostly the out-of-plane O $2p_x$ character, while the in-plane components O $2p_z$ and O $2p_y$ combine with H $1s$ and form the O—H bonding orbitals $3a_1$ and $1b_2$, respectively. The unoccupied orbitals $4a_1$ and $2b_2$ are the antibonding counterparts of these two orbitals. In the O $1s$ absorption spectrum of H_2O (Fig. 1, see also [14,15]) there are two broad resonances corresponding to the promotion of the O $1s$ orbital to the unoccupied molecular orbitals $4a_1$ and $2b_2$. In the present work, we focus on the latter O $1s \rightarrow 2b_2$ resonance.

II. EXPERIMENT

The experiments are carried out on a high-resolution plane grating monochromator installed in the c branch of the soft-x-ray figure-8 undulator beamline 27SU at SPring-8 [16–19]. The figure-8 undulator provides the linearly polarized light whose direction of the E vector for the first-order (0.5th-order) harmonic photon is horizontal (vertical). The
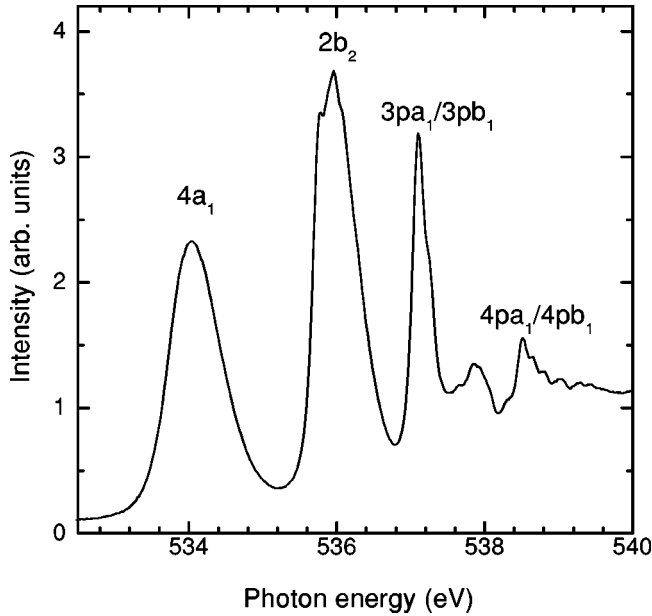
FIG. 1. The total ion yield spectrum of H_2O in the O $1s$ excitation region measured with ~55 meV bandwidth.

energy scale of the monochromator was calibrated by the use of O $1s$ to Rydberg transitions in CO_2.

The yield curves for mass selected ions are measured by use of a linear time-of-flight (TOF) mass spectrometer with a 690-mm-long drift tube [20]. An effusive beam of gaseous H_2O from the gas nozzle crosses with the photon beam at an ionization point on the TOF axis. The electrons and ions are extracted with the dc electric field of 1000 V/cm in opposite directions: the electron detection signals are used to start the time-to-digital converter (TDC), while the ion detection signals are used to stop the TDC. In this way the TOFs of all the fragment ions are measured simultaneously. The total ion yield curves of H_2O and D_2O are also measured. To do that, the polarity of the dc field is changed and the ions are detected, without mass selection, by the electron detector of the TOF spectrometer.

The angle-resolved yield curves for the energetic ions are measured by use of a pair of energetic-ion detectors placed horizontally and vertically, downstream of the TOF spectrometer along the incident photon beam and 250 mm apart from it [21]. Gaseous H_2O molecules are introduced coaxially with the photon beam by use of a coaxial gas nozzle positioned downstream. The measurements are carried out for both horizontal and vertical directions of the E vector. In this way the energetic-ion yield spectra $I(0°)$ and $I(90°)$ compensated for the difference in the detection efficiency of the two detectors are directly obtained. The retarding voltage used is 6 V and thus the H^+ ions with kinetic energies higher than 6 eV are detected.

III. RESULTS AND DISCUSSION

Figure 1 shows the total ion-yield spectrum of H_2O in the whole O $1s$ excitation region obtained with ~55 meV bandwidth. The broad bands at 534 eV ($4a_1$) and 536 eV ($2b_2$)

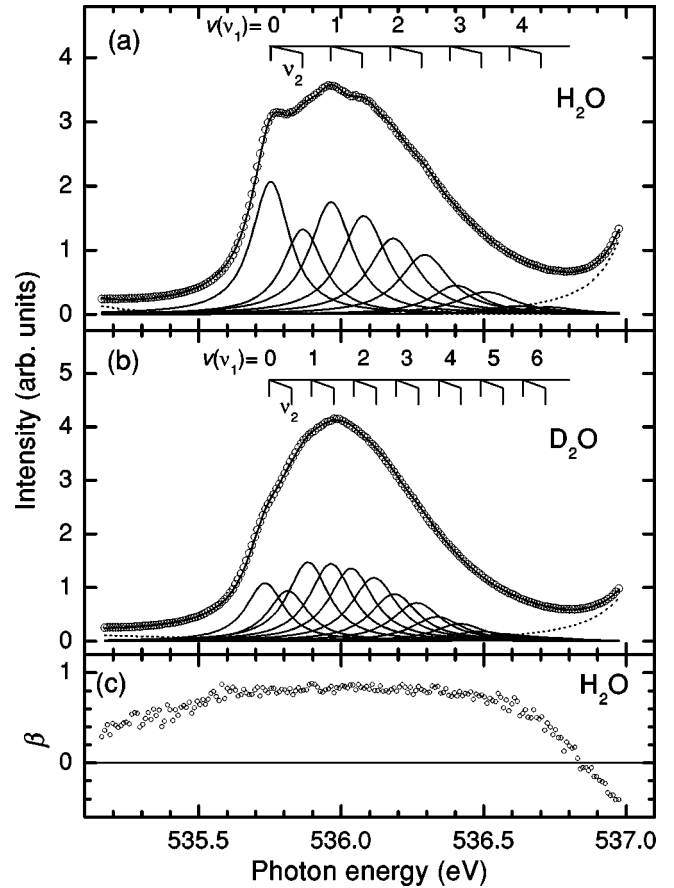FIG. 2. High-resolution (~40 meV) spectra of H_2O (a) and D_2O (b) in the region of the $2b_2$ band. The solid curves are the result of the least-squares peak fit. (c) The angular anisotropy parameter β for the energetic (≥ 6 eV) H^+ ions produced from H_2O.

are the promotions of the electron from O $1s$ to the unoccupied molecular orbitals $4a_1$ and $2b_2$, respectively, whereas the structures between 537 eV and 540 eV are the transitions to the Rydberg members [14,15,22]. Vibrational structures have never been observed so far either in the $4a_1$ or $2b_2$ band [15]. Actually, the O $1s \rightarrow 4a_1$ band shows no structure even under the present resolution, which is the highest ever achieved. This observation confirms the dissociative character of this state, as reported previously [15,23].

In contrast to $4a_1$, the $2b_2$ band clearly exhibits vibrational structures with obvious peaks at 535.74, 535.95, and 536.08 eV and a bump at 535.85 eV, as presented in the higher resolution spectrum (band pass ~40 meV) in Fig. 2(a). The vibrational structures become less clear in the higher energy side of the $2b_2$ band, suggesting that higher vibrational states may be dissociative. The observed vibrational structure cannot be explained by a simple progression of one vibrational mode. We therefore examine the symmetry characters of the transition involved. From the angle-resolved yield curves $I(0°)$ and $I(90°)$ for the energetic H^+ ions, the angular anisotropy parameter β is deduced using the relation $\beta = 2[I(0°) - I(90°)]/[I(0°) + 2I(90°)]$. The value of β thus obtained is ~0.8 in the entire range of the $2b_2$ resonance without any structure, as shown in Fig. 2(c). The value of $\beta \sim 0.8$ implies that the vibronic (electronic +

vibrational) symmetry should be B_2 [14,22]. Therefore, the observed vibrations should be symmetric stretching and/or bending in a_1 symmetry: if the antisymmetric stretching in b_2 symmetry were included, the vibronic symmetry of the transition would no longer be B_2.

To proceed with the analysis of the vibrational structure, a least-squares peak fitting is carried out for the entire $2b_2$ band. In the present peak fitting, two vibrational modes ν_1 and ν_2 both with constant vibrational spacings (harmonic approximation) are assumed and each peak is assumed as a convolution of a Gaussian profile with 40 meV full width at half maximum (FWHM) and a Lorentzian profile. It is assumed also that the FWHM of the Lorentizan profile has the lower limit value of 150 meV, i.e., the core-hole lifetime width [24], at the first peak at 535.74 eV, and increases linearly with the increase in the vibrational energy. The Lorentzian width as a function of vibrational energy E_{vib} is found to be $0.15 + 0.1E_{\text{vib}}$ (eV). This energy-dependent Lorentzian width is necessary for the reasonable fitting, suggesting that the higher vibrational states are indeed dissociative. The vibrational spacings obtained via fitting are $\nu_1 = 215 \pm 5$ meV and $\nu_2 = 114 \pm 5$ meV, as seen in Fig. 2(a). An even number of ν_2 vibrational states cannot be distinguished from the ν_1 sequence because the ν_1 frequency is about twice the ν_2 frequency. A similar analysis is carried out for D$_2$O, as shown in Fig. 2(b). The reasonable fitting is obtained for $\nu_1 = 151 \pm 5$ meV and $\nu_2 = 80 \pm 5$ meV using a frequency reduction factor 0.7 from H$_2$O to D$_2$O. The consistent fitting between H$_2$O and D$_2$O for the vibrational structures indicates the validity of our analysis and eliminates the possibility of the overlap of another electronic state in this resonance as previously suggested [14].

To understand the vibrational character of the observed vibrational modes in the $2b_2$ resonance, we have performed theoretical calculations on FH$_2$, relying on the equivalent-core approximation. The basis set used is aug-cc-pVTZ [25], for F and H: the f basis functions on fluorine are deleted and a p diffuse function ($\alpha = 0.025\,26$) on hydrogen is added. We have performed complete active space self-consistent-field (CASSCF) calculations using the MOLCAS package [26]. Active space is built on seven electrons in eight orbitals (three of a_1 symmetry, two of b_1, and three of b_2) while $1a_1^2$, and $2a_1^2$ are frozen, in order to describe both lone-pair correlation and excited states. According to the calculation, the O $1s^{-1}2b_2$ core-excited state, which is strongly mixed with the $3pb_2$ Rydberg character, has a C_{2v} stable geometry that is quite different from the ground state: the O—H bond is elongated by 0.25 Å and the H-O-H angle is 10° less. Similar deformation was reported in the calculation for H$_2$S, although the potential well is not deep enough to have vibrational states except the zero vibrational state [27]. Because of the large change of both the bond length and the bond angle, we can expect that both symmetric stretching and bending motions are caused by the O $1s \rightarrow 2b_2$ excitation. The vibrational frequencies in this stable geometry in O $1s^{-1}2b_2$ are estimated to be $\nu_1 = 186$ meV for the symmetric stretching vibration and $\nu_2 = 124$ meV for the bending vibration, in reasonable agreement with our experimental results for H$_2$O.
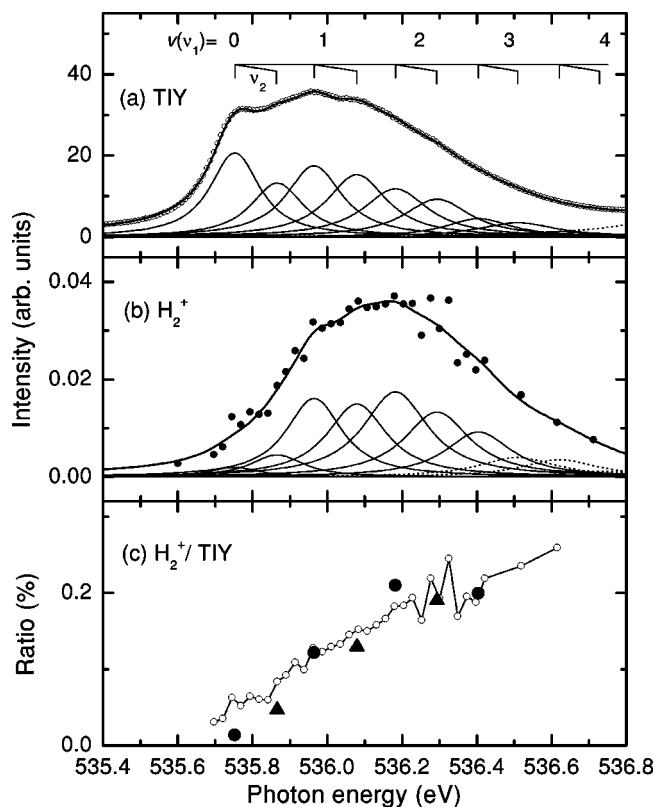

FIG. 3. The total ion yield spectrum (a) and the H$_2^+$ yield spectrum (b) in the O $1s^{-1}2b_2$ resonance. The ratio H$_2^+$ to the total ion is also given in (c): open circles, estimated from the yield curves in (a) and (b); closed circles and triangles, estimated from the area of each vibrational component in (a) and (b) obtained via a least-squares fit, for $(n,0,0)$ and $(n,1,0)$, respectively.

The symmetric stretching and bending motions are, however, strongly coupled and thus ν_1 and ν_2 have both symmetric stretching and bending characters.

Figure 3 shows the H$_2^+$ ion yield curve (b) and the intensity ratio H$_2^+$ (c) relative to the total ion given in (a), as a function of the excitation photon energy. The H$_2^+$ ion yield curve is analyzed also in the same way as the total ion curve and the intensity ratio H$_2^+$ to the total ion for each vibrational quantum state is also plotted in Fig. 3(c). We can clearly see that the branching ratio to the H$_2^+$ formation increases linearly with an increase in the nuclear motion energy stored in the O $1s^{-1}2b_2$ core-excited state. The fact that H$_2^+$ formation is independent of the excited vibrational mode (ν_1 or ν_2) is in accordance with our theoretical prediction that the symmetric stretching and bending motions are heavily mixed. The linear dependence of the H$_2^+$ formation on the nuclear motion energy of the core-excited state clearly demonstrates that the H$_2^+$ formation is induced by the nuclear motion in the core-excited state. It should be noted that the H$_2^+$ formation is a minor process compared to other channels such as the H$^+$ and OH$^+$ formations even at the $2b_2$ resonance and is hardly observed at the $4a_1$ resonance [13].

In order to reveal the relation between the nuclear motion in the core-excited state and the H$_2^+$ formation, one needs to

clarify the reaction pathway to the H_2^+ formation in the Auger final states. To do that we have carried out *ab initio* calculations for potential energy of the Auger final states. Here, we focus on the spectator Auger final state $1a_1^2 2a_1^2 1b_2^2 3a_1^2 2b_2^1 (2\,^2B_2)$ following the O $1s \rightarrow 2b_2$ excitation. Participator Auger final states with one positive hole on the $1b_1$, $3a_1$, or $1b_2$ orbital might be considered alternatively. However, the minimum energies of H_2O^+ belonging to these electronic states are (more than 3 eV) smaller than the product channel of $O + H_2^+$. To form H_2^+ from those participator Auger final states, the nuclear motion energy in the core-excited state must be sufficiently large or the nuclear bending motion must be quite highly excited before the Auger decay. This seems to be unrealistic in the process considered here. The calculations are performed by using MOLPRO [28] at the level of the multireference configuration-interaction theory with single and double excitations using full-valence CASSCF wave functions as references and employing the internally contracted configuration-interaction algorithm [29]. The aug-cc-pVTZ basis set of Dunning [25] is used. In the present theoretical analysis of the H_2^+ formation, we assume C_{2v} molecular symmetry. This is reasonable because H_2O^+ immediately dissociates into $OH^+ + H$ if the C_{2v} molecular symmetry does not hold. Potential-energy surfaces obtained by preliminary *ab initio* calculations with C_s molecular symmetry clearly showed strongly repulsive force along one of the O-H internuclear distances owing to the nonbonding $2b_2$ orbital. In Fig. 4 we show the potential energy curves of the spectator Auger final state of $H_2O^+(2\,^2B_2)$ as a function of the H-O-H angle. Both of the O-H internuclear distances r are fixed at some representative values. The figure clearly shows that H_2O^+ becomes much more stable energetically with the increase in the O-H distance and the decrease in the H-O-H angle. At $r \lesssim 4.5$ bohr, the potential curve has a deep well. At sufficiently larger r, the potential curve almost coincides with the diatomic H_2^+ potential. In fact, the depth of the potential well at $r = 8$ bohr is approximately equal to the dissociation energy of H_2^+ ($= 2.65$ eV). From these characteristic features of the potential energy curves, we expect that H_2O^+ possibly dissociates into $O + H_2^+$ and that this H_2^+ formation channel is promoted by the nuclear motion toward the smaller H-O-H angle and the larger O-H distance before the Auger decay. These theoretical analyses are in good accord with the experimental observations described above.

IV. CONCLUDING REMARK

We have observed the vibrational structures of the core-excited state of H_2O in which the O $1s$ electron is promoted to the $2b_2$ unoccupied molecular orbital. On the ground of the observed vibrational structures and the theoretical investigation of the potential surface of the core-excited state, we have confirmed that the O $1s \rightarrow 2b_2$ excitation of H_2O causes the bending motion mixed with the symmetric stretching motion. Also we found that the H_2^+ formation along the Auger final states in H_2O^+ increases linearly with the vibrational en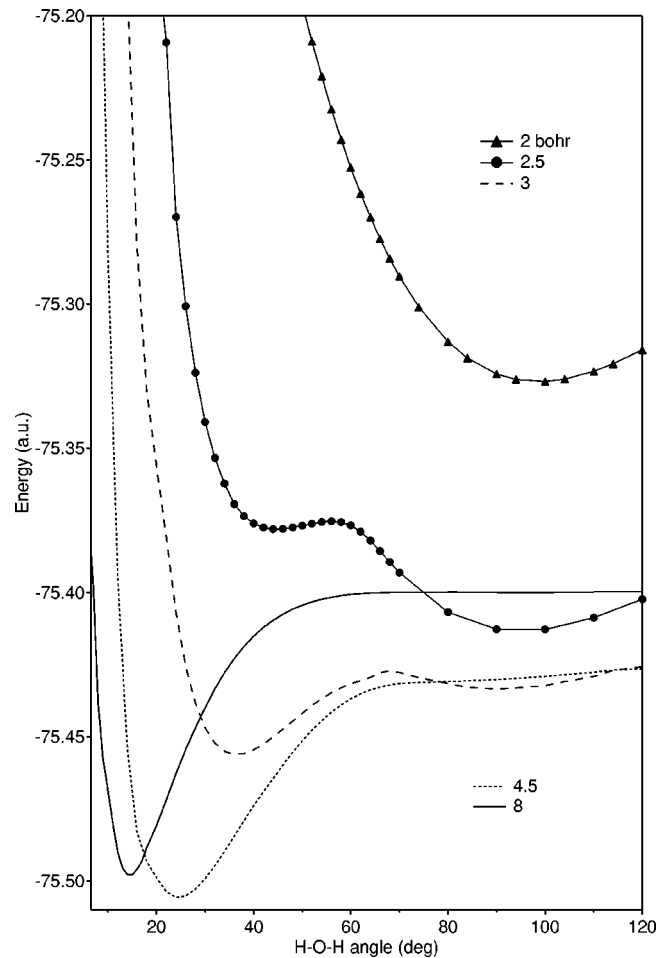ergy stored in the core-excited state. The *ab initio* calculations of the Auger final states leading to the H_2^+ formation suggest clearly that the nuclear motion before the Auger decay plays a key role.

FIG. 4. Potential-energy curves of the spectator Auger final state ($1a_1^2 2a_1^2 1b_2^2 3a_1^2 2b_2^1 ; 2\,^2B_2$) as a function of the H-O-H angle. The calculations are carried out keeping C_{2v} molecular symmetry. Both of the O-H internuclear distances are fixed at some representative values.

[1] F.X. Gadea, H. Köppel, J. Schirmer, L.S. Cederbaum, K.J. Randall, A.M. Bradshaw, Y. Ma, F. Sette, and C.T. Chen, Phys. Rev. Lett. **66**, 883 (1991).

[2] G. Remmers, M. Domke, and G. Kaindl, Phys. Rev. A **47**, 3085 (1993).

[3] N. Kosugi, J. Electron Spectrosc. Relat. Phenom. **79**, 351 (1996), and references cited therein.

[4] M. Neeb, J.E. Rubensson, M. Biermann, and W. Eberhardt, J. Electron Spectrosc. Relat. Phenom. **67**, 261 (1994).

[5] E. Kukk, H. Aksela, S. Aksela, F.K. Gel'mukhanov, H. Ågren, and S. Svensson, Phys. Rev. Lett. **76**, 3100 (1996).

[6] S. Sundin, F.Kh. Gel'mukhanov, H. Ågren, S.J. Osborne, A. Kikas, O. Björneholm, A. Ausmees, and S. Svensson, Phys. Rev. Lett. **79**, 1451 (1997).

[7] M. Simon, C. Miron, N. Leclercq, P. Morin, K. Ueda, Y. Sato, S. Tanaka, and Y. Kayanuma, Phys. Rev. Lett. **79**, 3857 (1997).

[8] K. Ueda, J. Electron Spectrosc. Relat. Phenom. **88-91**, 1 (1998), and references cited therein.

[9] W. Eberhardt, T.K. Sham, R. Carr, S. Krummacher, M. Strongin, S.L. Weng, and D. Wesner, Phys. Rev. Lett. **50**, 1038 (1983).

[10] C. Miron, M. Simon, N. Leclercq, D.L. Hansen, and P. Morin, Phys. Rev. Lett. **81**, 4104 (1998).

[11] K. Ueda, M. Simon, C. Miron, N. Leclercq, R. Guillemin, P. Morin, and S. Tanaka, Phys. Rev. Lett. **83**, 3800 (1999).

[12] P. Morin, M. Simon, C. Miron, N. Leclercq, E. Kukk, J.D. Bozek, and N. Berrah, Phys. Rev. A **61**, 050701 (2000).

[13] M.N. Piancastelli, A. Hempelmann, F. Heiser, O. Gessner, A. Rüdel, and U. Becker, Phys. Rev. A **59**, 300 (1999).

[14] D.Y. Kim, K. Lee, C.I. Ma, M. Mahalingam, D.M. Hanson, and S.L. Hulbert, J. Chem. Phys. **97**, 5915 (1992).

[15] J. Schirmer, A.B. Trofimov, K.J. Randall, J. Feldhaus, A.M. Bradshaw, Y. Ma, C.T. Chen, and F. Sette, Phys. Rev. A **47**, 1136 (1993).

[16] T. Tanaka and H. Kitamura, J. Synchrotron Radiat. **3**, 47 (1996).

[17] E. Ishiguro, H. Ohashi, Li-jun Lu, W. Watari, M. Kamizato, and T. Ishikawa, J. Electron Spectrosc. Relat. Phenom. **101-103**, 979 (1999).

[18] H. Ohashi, E. Ishiguro, Y. Tamenori, H. Okumura, A. Hiraya, H. Yoshida, Y. Senba, K. Okada, N. Saito, I.H. Suzuki, K. Ueda, T. Ibuki, S. Nagaoka, I. Koyano, and T. Ishikawa, Nucl. Instrum. Methods A (SRI2000 proceedings) (to be published).

[19] H. Ohashi and Y. Tamenori, SPring-8 Information **5**, 256 (2000) (in Japanese).

[20] I. Koyano, M. Okuyama, E. Ishiguro, A. Hiraya, H. Ohashi, T. Kanashima, K. Ueda, I.H. Suzuki, and T. Ibuki, J. Synchrotron Radiat. **5**, 545 (1998).

[21] K. Ueda, H. Yoshida, Y. Senba, K. Okada, Y. Shimizu, H. Chiba, H. Ohashi, Y. Tamenori, H. Okumura, N. Saito, S. Nagaoka, A. Hiraya, E. Ishiguro, T. Ibuki, I.H. Suzuki, and I. Koyano, Nucl. Instrum. Methods A (SRI2000 proceedings) (to be published).

[22] K. Okada, K. Ueda, T. Tokushima, Y. Senba, H. Yoshida, Y. Shimizu, M. Simon, H. Chiba, H. Okumura, Y. Tamenori, H. Ohashi, N. Saito, S. Nagaoka, I.H. Suzuki, E. Ishiguro, I. Koyano, T. Ibuki, and A. Hiraya, Chem. Phys. Lett. **326**, 314 (2000).

[23] A. Naves de Brito, R. Feifel, A. Mocellin, A.B. Machado, S. Sundin, I. Hjelte, S.L. Sorensen, and O. Björneholm, Chem. Phys. Lett. **309**, 377 (1999).

[24] A. Cesar, H. Ågren, and V. Carravetta, Phys. Rev. A **40**, 187 (1989).

[25] T.H. Dunning, Jr., J. Chem. Phys. **90**, 1007 (1989).

[26] K. Andersson *et al.*, *MOLCAS Version 4.1* (Lund University, Sweden, 1997).

[27] A. Naves de Brito and H. Ågren, Phys. Rev. A **45**, 7953 (1992).

[28] MOLPRO is a package of *ab initio* programs written by H.-J. Werner and P.J. Knowles, with contributions from R.D. Amos *et al.*

[29] H.-J. Werner and P.J. Knowles, J. Chem. Phys. **89**, 5803 (1988); P.J. Knowles and H.-J. Werner, Chem. Phys. Lett. **145**, 514 (1988).